Armenian Journal of Physics, 2024, vol. 17, issue 3, pp. 58-64

Determination of Photoneutron Production from Different Targets Irradiated by Electron Beam

E. Melyan, K. Katovský, S. Mukherjee

Department of Electrical Power Engineering, Brno University of Technology, Technická 3082/12 T12, 616 00 Brno, Czech Republic

E-mail: melyan@vutbr.cz

(Received: October 12, 2024; Revised: November 10, 2024; Accepted: November 28, 2024)

Abstract. In the present work, a study has been conducted to estimate the production of photoneutrons from different targets irradiated by a 70 MeV electron beam. The linear electron accelerator at the Yerevan Physics Institute in Armenia was used for the purpose. The reaction rates were determined through detailed off-line analysis of experimental data and subsequently compared to theoretical predictions by using the MCNP (Monte Carlo N-Particle Transport) and Cascade Exciton Physics Model (CEM03.03) codes.

Keywords: photoneutron, reaction rates, electron beam, MCNP code, CEM03.03 code

DOI: 10.54503/18291171-2024.17.3-58

1. Introduction

There are many approaches to produce neutrons including fission reactors, alpha neutron sources, spontaneous fission neutron sources, accelerators. Out of these options nuclear fission reactors offer the highest neutron flux, however, they are neither widely accessible nor simple to construct [1]. Alpha neutron sources are also unsuitable for many practical applications having limited neutron flux, significant safety risks from radioactive materials and short operational lifespan. Spontaneous fission neutron sources on the other hand can provide higher neutron fluxes however sharing the same disadvantages as the latter. In contrast, electron LINAC-based neutron sources are compact, economical, reliable, easy to handle and most suitable for neutron applications. Advances in accelerator technology have made these systems more efficient, and safer, using non-radioactive materials. These features make linac-based neutron sources highly attractive for nuclear and materials research. This approach produces neutrons primarily through bremsstrahlung processes, where the high-energy electron beams interacting with heavy target materials generate gamma rays. The gamma rays induce photoneutron reactions when their energy surpasses a specific threshold, triggering photonuclear reactions that result in the release of neutrons.

Reaction rates are one of the important properties of nuclear reactions essential for understanding and optimizing the neutron production, distribution and overall behavior of the nuclear system such as accelerator driven system (ADS) [2-3]. These rates directly impact the reactors' performance including fuel efficiency, waste transmutation and safety.

The primary objective of this work is to analyze and characterize photoneutron production from various target materials exposed to high-energy electron beam irradiation. The study involves identifying the dependence of photoneutron yields on the type of target material, electron beam energy, and irradiation conditions. By combining experimental measurements with the theoretical modeling, the work will lead towards the understanding of photoneutron production processes. This will contribute to the development of optimized target materials for various applications and to the assessment of radiological safety concerns associated with high-energy electron beam systems.

2. Experimental set up

This research focused on determining photoneutron production using BeO photoneutron converter, which were chosen because of low threshold energy and high (γ, n) cross section properties. There are two primary processes involved: the interaction of high-density tungsten with bombarding electrons, which produces bremsstrahlung radiation, and the subsequent interaction of photons with a BeO converter, which generates neutrons. The experiment was performed on a linear electron accelerator [4] at the Yerevan Physics Institute in Armenia. A set of targets as mentioned in table 1, was irradiated by 70 MeV electron beam with intensity of 5.61×10^{12} particles per second. Irradiation lasted for a duration of 3.06 hours with all targets together. A schematic diagram of the experiment is shown in Fig.1.

The electron beam was directed on 0.5 mm thick and 125 mm^2 surface area tungsten foil for photon conversion, aluminum cylinder with identical dimensions, proposed for additional stopping of electrons, and aluminum foil for beam monitoring has been used. Table 1 presents the activation samples irradiated in the experiments with the same 12.5×12.5 mm dimensions.

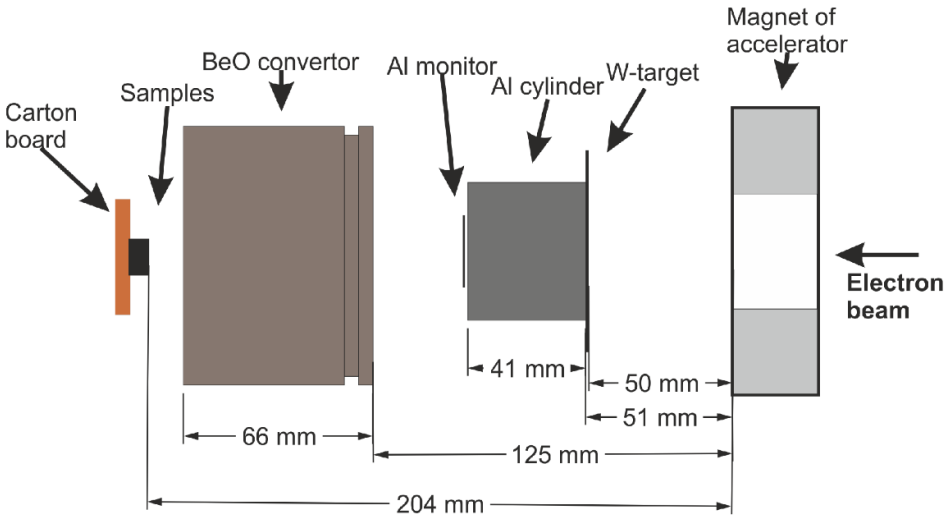

Fig. 1. Schematic diagram of the experimental setup.

Table 1. Thickness and weights of the samples being used in the experiment.

Material	Molar Mass	Thickness, (mm)	Weight, (g)
Al	26.98	0.5	0.2150
Y	88.91	0.25	0.1641
V	50.94	0.25	0.2248
In	114.82	0.1	0.1060
Co	58.93	0.5	0.7174
Cu	63.55	0.125	0.4019
Bi	208.98	0.5	0.7276
Ta	180.95	0.125	0.3069
Au	196.97	0.0125	0.0401
Nb	92.91	0.5	0.3341
Mn	54.94	0.05	0.0982

3. MCNP simulation

The experiment was modeled identical to the above described setup by MCNP 6.2 [5] software simulating photonuclear processes. Fig.2 shows the complete model with all the cells

enclosed in the air sphere cell, where three tungsten, aluminum and converter are visible in addition to aluminum monitor foil hidden in between. The other enlarged section shows activation foils that are not visible in the full image.

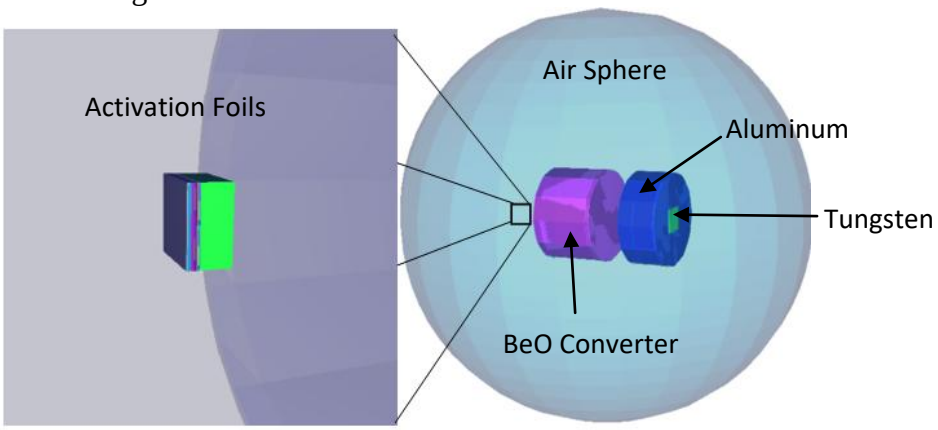

Fig. 2. Geometrical model of MCNP simulation.

The default Cascade Exciton Physics Model (CEM03.03) was used for the calculation. The model calculates a variety of nuclear reaction properties, including total reaction and fission cross-sections, excitation functions, nuclide yield distributions, energy and angular spectra, etc. As specified in the user manual [6], the model is best suited for the energy ranges between approximately 10 MeV and 5 GeV. The electron beam was modeled perpendicular to the 1 cm diameter targets, uniformly and monodirectionally, emitting electrons with radial sampling from a circular surface. The calculations were done for 10^9 particle histories. For thermal treating the free gas model was involved [7] with cross section for BeO converter from $S(\alpha,\beta)$ libraries corresponding to the room temperature [8]. The material compositions were set according to the PNNL reference document [8]. The continuous energy cross sections used in the model are taken from "ENDF71x", "el", "la150u" libraries for neutron, electron and photonuclear data respectively [7].

4. Results and discussion

As a result of the investigation of various target materials under irradiation, both experimentally and theoretically, certain reaction rates have been obtained and compared. In addition, the modeled simulations computed neutron fluxes in activation foils and total photoneutron production, along with their corresponding flux properties were also compared. The experimental results were obtained using the method of induced activity used for the reaction rate calculations. The technique is widely used due to its ability to detect elements at lower boundaries. The current work involves the activation of the material with neutrons, gamma quanta or charged particles, resulting in excited nuclei or radioactive isotopes, which is particularly advantageous for studying the production mechanisms of residual nuclei over a wide mass range.

The γ-ray spectra of irradiated samples were measured with high-purity germanium (HPGe) detector [10] in the underground salt mine, in low background laboratory at the depth of 240 meters. The processing of the measured data was carried out using the DEIMOS32 code package in an off-line analysis [11]. A typical γ-ray spectrum obtained using a 59Co target is shown in Fig.3. The high intensity of these peaks compared to the background demonstrates the efficiency of the HPGe detector in resolving gamma-ray energies. Among the various peaks observed in the spectrum the graph highlights two 810.6 keV and 1674.5 keV energy channels, which confirms the characteristic gamma emissions expected under these conditions.

The experimental reaction rates were obtained using the relation given in equation (1)

$$R_R = \frac{Q \cdot t_{irr}}{N_T \cdot I_P} \quad (1)$$

where t_{irr} is the total time of irradiation, N_T is the number of atoms in the measured sample, I_P is the integral number of particles and Q is the production rate. The latter is given by the equation (2)

$$Q = A_0 \cdot \frac{\lambda \cdot t_{irr}}{1-\exp(-\lambda \cdot t_{irr})} \quad (2)$$

where A_0 is the activity at the end of the irradiation and λ is the decay constant. The calculated reaction rates are presented in Table 3.

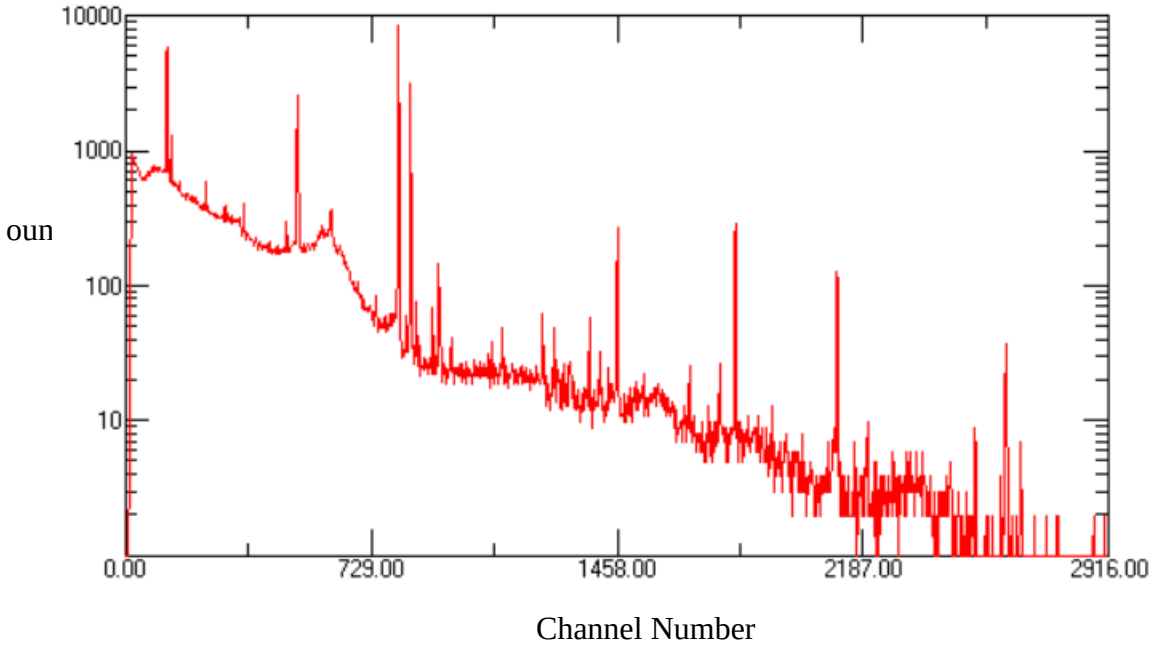

Fig. 3. A typical gamma-ray spectrum for ^{59}Co target.

The result of the MCNP code calculations showed several important nuclear properties of the experiment. Given a 0.9 μA current (5.61×10^{12} electrons/second), 1.52×10^{10} neutrons/second source strength was calculated. The average of all neutrons energies was found to be 2.5 MeV. The average number of neutrons produced per photonuclear absorption is calculated to be 0.82.

Table 2 shows the neutron flux for each single activation foil, calculated using F4 tally in the code, which is the averaged flux over a cell. It is important to note that the values presented in the table are those corresponding to one source particle, i.e. for instance for niobium, 7.5 neutrons are produced for every 1000 incident electrons. The lowest neutron flux was obtained for aluminum foil, due in part to the high threshold energy of the reaction.

Table 2. Neutron flux in foils per incident particle.

Material	Flux [neutrons/cm^2/electron]	Material	Flux [neutrons/cm2/electron]
Nb	7.56E-03 ±0.0278	Mn	6.93E-04 ±0.0478
Ta	7.99E-04 ±0.0426	Co	6.70E-04 ±0.0442
Y	7.36E-04 ±0.0418	Bi	6.32E-04 ±0.0471
Al	7.14E-08 ±0.0446	In	5.94E-04 ±0.0629
Cu	7.04E-04 ±0.0456	Au	5.34E-04 ±0.0546
		Total	1.76E-03 ±0.0256

Reaction rates in the MCNP software were calculated using the FM tally multiplier with the atomic density and reaction type number taken from the reference [12]. This entry gives reaction rate results with corresponding error.

The visualizations of photon and neutron fluxes are presented in Fig.4, which clearly shows that along the pathway of the electron beam photons are created for every source particle. In the second profile picture the neutrons tracks are seen originating from material cells as expected. It is a matter of discussion why the BeO converter cell appears with rather few neutrons, while the aluminum cylinder placed in front of it appears with more. The explanation may be the weakness of the MCNP software in modeling photonuclear phenomena.

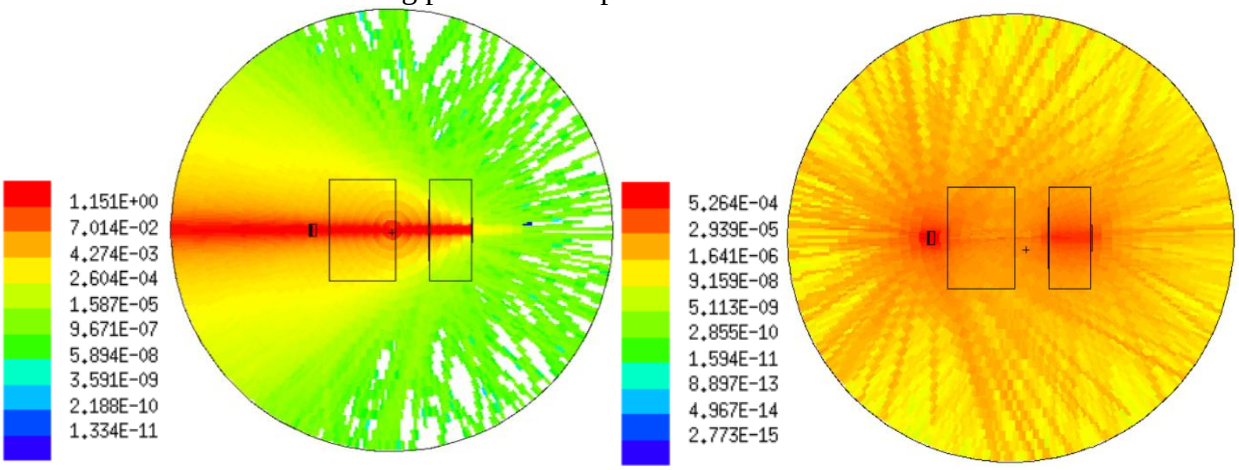

Fig. 4. Photon and neutron fluxes visualization in particles/cm^2/electron units.

Table 3 shows the calculated reaction rates for each irradiated material target, according to which the experimental values are higher for all the cases compared to the corresponding predicted ones. However, the values of some materials for certain reaction types were in good agreement, e.g., the (n, α) reaction rates for Co or the (n, γ) reaction rates for Cu, In, Au. Those reactions present in both studies are visualized in the form of graphs shown in Fig. 5-6, where the differences are clearly visible, especially for (n, α) and (n, 2n) reactions.

Table 3. Reaction rates obtained from experimental and theoretical calculations.

Material	Reaction Type	Reaction Rate Experiment [atom^{-1}s^1]	Error	Reaction Rate Simulation [atom^{-1}s^1]
Nb	(n,2n)	4.24E-28	0.0574	3.30E-30
Ta	(n,α)	9.77E-29	0.0125	3.50E-33
	(n,2n)	9.49E-28	0.0118	6.99E-30
Y	(n,α)	1.12E-29	0.014	1.40E-32
	(n,2n)	9.26E-28	0.0165	1.36E-30
	(n,3n)	7.32E-29	0.0919	-
Al	(n α)	1.11E-30	0.0144	4.40E-31
Cu	(n,γ)	2.11E-30	0.0269	5.42E-30
	(n,3n)	2.25E-29	0.0428	-
Mn	(n,γ)	6.20E-31	0.0668	7.94E-30
	(n,2n)	6.42E-31	0.0251	1.42E-30
Co	(n, α)	8.91E-31	0.0473	8.90E-31
	(n,2n)	2.91E-28	0.0483	1.04E-30
	(n,3n)	5.93E-29	0.0211	-
Bi	(n, α)	6.54E-29	0.0839	2.40E-33
In	(n, α)	1.95E-30	0.0254	4.50E-33
	(n,p)	1.67E-30	0.0216	1.55E-32
	(n,γ)	1.64E-29	0.0225	8.03E-29

	(n,3n)	1.53E-29	0.0192	9.94E-32
Au	(n, α)	5.59E-29	0.0898	2.30E-33
	(n,γ)	1.97E-29	0.0255	1.97E-29
	(n,2n)	2.40E-27	0.0352	4.93E-30

It can be seen in Fig.5 and 6 for (n, α) reaction, the theoretical calculations underestimate the experimental results. This is obvious, since alpha emission in particular involves cluster formation, which depends on both quantum mechanics and collective effects. Many models, including CEM03.03, treat alpha emission semi-classically, potentially overestimating the probability of alpha particle formation. This can cause the (n, α) reaction cross-sections to be higher than the experimental results Use of advanced cluster models or empirical corrections for alpha emission probabilities may be a better solution. Similarly, in reaction (n, 2n), the parameters in these models, such as potential depth or radius, may not be fully optimized for certain nuclei. This can lead to an overprediction of the outgoing particle flux, especially in secondary particle production. In addition, the exciton model predicts excessive secondary neutron emission in pre-equilibrium mode. This simplified cascade energy distribution increases the neutron ejection cross section. In the present work, the parameters in CEM03.03 are globally optimized, i.e. they are designed to work for a wide range of isotopes and reactions. This may result in inaccuracies for certain isotopes or reaction types like (n, 2n).

The calculation of the (n, γ) reaction with CEM03.03 physical model is due to the limited treatment of the competition between gamma emission and particle ejection. The code does not accurately represent nuclear states, thereby reducing the probability of gamma emission. It can be conservatively stated that the model favors particle emission over gamma transitions. Therefore, the theoretical calculations generally underestimate the experimental results.

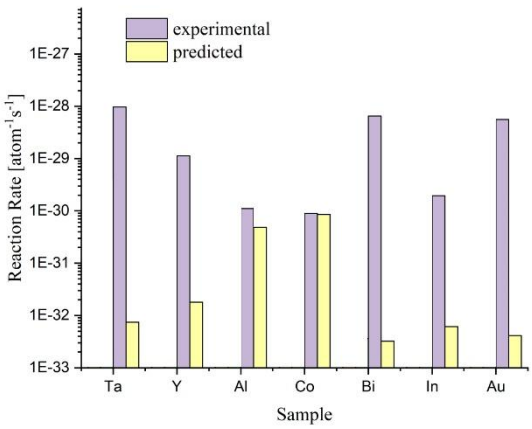

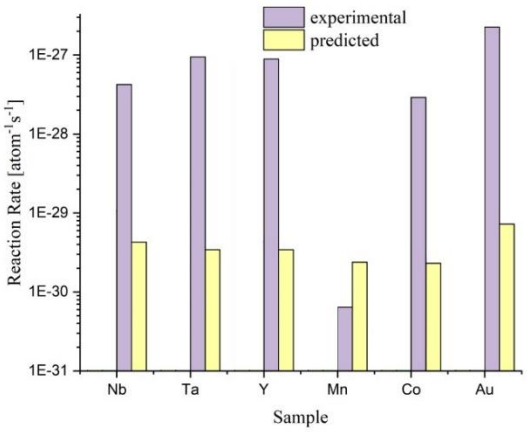

Fig. 5. Experimental and theoretical results of (n, α) and (n, γ) reaction rates.

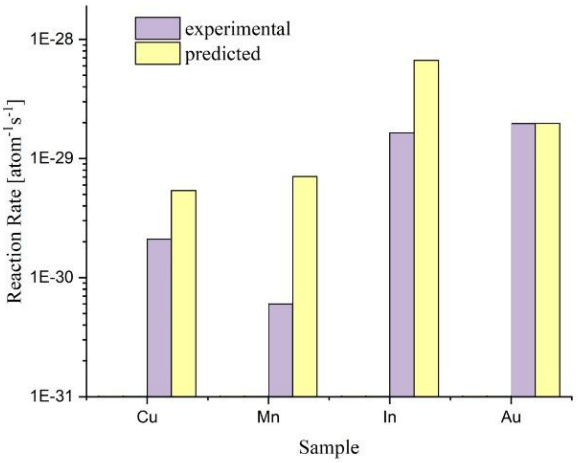

Fig. 6. Experimental and theoretical results of (n, 2n) reaction rates.

5. Conclusions

In the current study, the reaction rates, neutron fluxes, and photoneutron production properties were investigated for various target materials using both experimental and theoretical methods. The common reaction rates for all cases were compared and presented in tables and graphs. Results calculated using the simulation code showed an underestimation compared to experimental data, although some close matches were observed for specific materials and reaction types. Overall, most values showed significant deviations, likely due to the limitations of the MCNP software in accurately modeling photonuclear phenomena, as indicated by graphs and neutron flux visualizations. The CEM03.03 code calculations demonstrate significant deviations from the experimental results due to the limitations of the semi-classical structure of the code.

References

[1] D. Schlissel, B. Biewald, Nuclear Power Plant Construction Costs (Synapse Energy Economics, Inc., 2008).
[2] H. Nifenecker, O. Meplan, S. David, Accelerator Driven Subcritical Reactors (IOP Publishing Ltd, Bristol, 0 7503 0743 9, 2003).
[3] H. Feizi, A.H. Ranjbar, J. Instrumentation **11** (2016) P02004.
[4] A. Sirunyan, A. Hakobyan, G. Ayvazyan, A. Babayan, H. Vardanyan, G. Zohrabyan, K. Davtyan, H. Torosyan, A. Papyan, J. Contemp. Phys. **53** (2018) 271.
[5] C.J. Werner, MCNP User's Manual - Code (Version 6.2, Los Alamos National Laboratory, 2017).
[6] S.G.Mashnik, A.J. Sierk, CEM03.03 User Manual (LANL report LA-UR-12-01364, 2002).
[7] E.E. Sunny, Temperature Effects of Resonance Scattering for Epithermal Neutrons in MCNP (Los Alamos National Laboratory, LA-UR-11-06503, 2012).
[8] J.L. Conlin, Linsting of Available ACE Fatat Tables (Los Alamos National Laboratory, report LA-UR-17-20709, 2017).
[9] R.J. McConn, C.J. Gesh, R.T. Pagh, R.A. Rucker, R.G. Williams, Compendium of Material Composition Data for Radiation Transport Modeling (Revision 1, Pacific Northwest National Laboratory Richland, Washington, 2011).
[10] Hyper-Pure Germanium Detector, Radioisotopes and Radiation Methodology, Med. Phys. 4RA3, 4RB3/6R03, 1999.
[11] J. Frana, J. Radioanal. Nucl. Chem. **257** (2003) 583.
[12] M. Herman, ENDF-6 Formats (Report BNL-90365-2009 Rev.1, Brookhaven National Laboratory, 2010).